Dalton Transactions

Mechanistic Investigation of the Aerobic Oxidation of 2-pyridylacetate Coordinated to a Ru(II) Polypyridyl Complex

Journal:	*Dalton Transactions*
Manuscript ID	DT-ART-07-2021-002461.R2
Article Type:	Paper
Date Submitted by the Author:	27-Sep-2021

Complete List of Authors:	Fernandes Sousa, Sinval; Universidade Federal de Uberlandia, Quimica Ertem, Mehmed Z.; Brookhaven National Laboratory, Chemistry Department Faustino, Leandro; Universidade Federal de Uberlandia Instituto de Quimica Machado, Antonio; Universidade Federal de Uberlandia, Instituto de Química Concepcion, Javier; Brookhaven National Laboratory, Chemistry da Silva Maia, Pedro; Universidade Federal do Triangulo Mineiro, Chemistry Patrocinio, Antonio; Universidade Federal de Uberlandia Instituto de Quimica,

Mechanistic Investigation of the Aerobic Oxidation of 2-pyridylacetate Coordinated to a Ru(II) Polypyridyl Complex†

Sinval F. Sousa[1], Mehmed Z. Ertem[2,*], Leandro A. Faustino[1], Antonio Eduardo. H. Machado[1], Javier J. Concepcion[2], Pedro I. S. Maia[3], Antonio Otavio T. Patrocinio[1,*]

[1] Laboratory of Photochemistry and Materials Science, Institute of Chemistry, Universidade Federal de Uberlandia, 38400-902, Uberlandia, Brazil

[2] Chemistry Division, Energy & Photon Sciences Directorate, Brookhaven National Laboratory, Upton, USA

[3] Núcleo de Desenvolvimento de Compostos Bioativos (NDCBio), Universidade Federal do Triângulo Mineiro, Av. Dr. Randolfo Borges 1400, 38025-440 Uberaba, MG, Brazil

*To whom the correspondence should be addressed:
otaviopatrocinio@ufu.br
mzertem@bnl.gov

†Electronic supplementary information (ESI) available. See DOI: XXX

Abstract

A new ruthenium polypyridyl complex, $[Ru(bpy)_2(acpy)]^+$ (acpy = 2-pyridylacetate, bpy = 2,2'-bipyridine), was synthesized and fully characterized. Distinct from the previously reported analog, $[Ru(bpy)_2(pic)]^+$ (pic = 2-pyridylcarboxylate), the new complex is unstable under aerobic conditions and undergoes oxidation to yield the corresponding α-keto-2-pyridyl-acetate (acpyoxi) coordinated to the Ru^{II} center. The reaction is one of the few examples of C-H activation at mild conditions using O_2 as the primary oxidant and can provide mechanistic insights with important implications for catalysis. Theoretical and experimental investigations of this aerobic oxidative transformation indicate that it takes place in two steps, first producing the α-hydroxo-2-pyridyl-acetate analog and then the final product. The observed rate constant for the first oxidation was in the order of 10^{-2} h^{-1}. The reaction is hindered in the presence of coordinating solvents indicating the rule of the metal center in the process. Theoretical calculations at the M06-L level of theory were performed for multiple reaction pathways in order to gain insights into the most probable mechanism. Our results indicate that O_2 binding to $[Ru(bpy)_2(acpy)]^+$ is favored by the relative instability of the six-ring chelate formed by the acpy ligand and the resulting Ru^{III}-$OO^{\bullet-}$ superoxo is stabilized by the carboxylate group in the coordination sphere. C-H activation by this species involves high activation free energies ($\Delta G^{\ddagger}$= 41.1 kcal mol^{-1}), thus the formation of a diruthenium μ-peroxo intermediate, $[(Ru^{III}(bpy)_2(O\text{-}acpy))_2O_2]^{2+}$ via interaction of a second $[Ru(bpy)_2(acpy)]^+$ was examined as an alternative pathway. The dimer yields two Ru^{IV}=O centers with a low $\Delta G^{\ddagger}$ of 2.3 kcal mol^{-1}. The resulting Ru^{IV}=O species can activate C-H bonds in acpy ($\Delta G^{\ddagger}$ = 23.1 kcal mol^{-1}) to produce the coordinated α-hydroxo-2-pyridylacetate. Further oxidation of this intermediate leads to the α-keto-2-pyridyl-acetate product. The findings provide new insights into the mechanism of C-H activation catalyzed by transition-metal complexes using O_2 as sole oxygen source.

Keywords: C-H activation; aerobic oxidation; O_2 activation; dehydrogenation reactions.

Introduction

The use of molecular oxygen as sole oxidant in the dehydrogenation of organic substrates has been the aim of intensive studies in recent years due to its potential as a green alternative to the traditional oxidation methods employing hazardous or toxic reagents.[1-4] Generally, molecular oxygen is employed as the terminal oxidant and the oxidation of the organic substrate is carried out by a redox mediator. For example, Anson et al.[5] have shown the role of Co^{II}(salophen) complex in the aerobic Pd-catalyzed allylic acetoxylation of cycloalkenes in the presence of hydroquinone as the redox mediator. In this system, the Co^{II} complex promotes the reduction of O_2 to yield Co^{III}-superoxide species, which further promotes the H-atom abstraction from hydroquinone. The resulting semiquinone radical undergoes oxidation by Co^{III}-hydroperoxide species to generate the reactive *p*-benzoquinone, which then acts as an effective oxidant in the Pd^0 surface. Other examples include oxidation of alcohols to the corresponding aldehydes or ketones employing Pd^{II} [6, 7], Cu^{I} [8-10] and Ru^{II} [11-13] based systems and hydroquinones or TEMPO (2,2',6,6'-tetramethylpiperidine) as co-catalysts. In most cases, metal-oxo (*M*=*O*) or metal-superoxo ($M\text{-}O_2^{\bullet-}$) species are identified as key intermediates in the catalytic cycle.

Other few attempts reported the aerobic oxidation of alcohols,[14] imidazolines[15, 16] and amines[17] employing Ru^{II} molecular catalysts without any other additives. These strategies are economically and environmentally attractive, but requires activation of molecular O_2 to act as the primary oxo-transfer agent and yield the effective catalytic species, Ru^{IV}=O or Ru^{V}=O. Formation of Ru^{IV}=O under mild conditions have typically been achieved by chemical or electrochemical oxidation of Ru^{II}-aquo complexes through proton-coupled electron transfer (PCET) reactions[18] and further explored for the development of molecular water oxidation catalysts.[19-23] So far, little attention has been given to the mechanistic aspects of O_2 reduction by Ru^{II} complexes, which could have important implications in catalysis.

In the present work, we report the reactivity of a new Ru(II) bis(bipyridine) complex containing the 2-pyridylacetate (acpy) ligand. This relatively simple compound undergoes oxidation by O_2 leading to the dehydrogenation of methylene protons of the acpy ligand to yield the α-oxo-acetate derivative

through an intramolecular C-H activation, Scheme 1. The system can be probed by spectroscopic techniques, allowing the identification of key reaction intermediates. Theoretical and experimental investigations carried out here allowed to identify the possible pathways for O_2 activation as well as the following C-H activation. The results provide fundamental insights into the Ru^{IV}=O chemistry with possible implications not only in aerobic oxidations catalyzed by metal complexes but also to the possible degradation mechanisms of Ru(II)-based water oxidation catalysts.

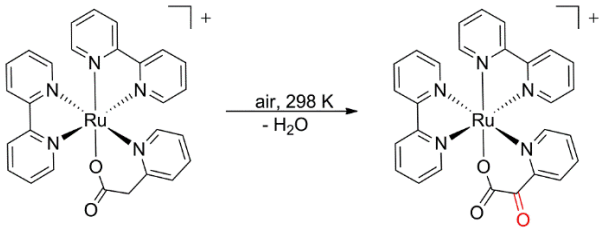

Scheme 1. Oxidation of the coordinated 2-pyridylacetate ligand in $[Ru(bpy)_2(acpy)]^+$ (acpy = 2-pyridylacetate, bpy = 2,2'-bipyridine) in the presence of O_2.

Experimental Methods

All solvents were HPLC grade. $RuCl_3$, *tert*-butylammonium hexafluorophosphate ($TBAPF_6$), 2,2'-bipyridine, 2-pyridylcarboxylic acid (Hpic), 2-pyridylacetic acid (Hacpy) hydrochloride were purchased from Aldrich and used without further purifications.

Synthesis. The complexes were prepared following a similar procedure reported previously.[24] 0.200 g (0.34 mmol) of the precursor *cis*-$[RuCl_2(bpy)_2].2H_2O$[25] were mixed with 0.06 mL (0.5 mmol) of triethylamine and 0.60 mmol of the selected carboxylic acid (Hpic or Hacpy**.**HCl) in (1:1) water/methanol mixture. The reaction mixture was kept under reflux for two hours under inert atmosphere. The volume was then reduced to half and NH_4PF_6 was added to precipitate the desired product. The products were separated by filtration, washed with cold water and ether, and dried under reduced pressure. For $[Ru(bpy)_2(acpy)]PF_6$, the as obtained powder was stored under *vacuum*.

$[Ru(bpy)_2(pic)]PF_6$: Yield 93%. Calculated elemental analysis for $C_{26}H_{20}O_2N_5PF_6Ru$ was C, 45.89%; N, 10.29%; H, 2.96%; *found:* C, 45.70%; N,

10.37%; H, 2.81%. Theoretical M^+: 536.0660 (100%); *found:* 536.0655 (100%). ^1H NMR ($(CD_3)_2CO$ δ / ppm): 8.92 (d, 1H); 8.75 (d, 2H); 8.68 (t, 2H); 8.14 (m, 5H); 8.00 (m, 3H); 7.82 (m, 2H); 7.72 (d, 1H); 7.62 (t, 1H); 7.47(t, 1H); 7.42 (dd, 2H).

$[Ru(bpy)_2(acpy)]PF_6$: Yield 94%. Calculated elemental analysis for $C_{27}H_{22}O_2N_5PF_6Ru.4H_2O$ was C, 41.54%; N, 8.97%; H, 3.62%; *found:* C, 41.98%; N, 8.94%; H, 3.75%. ESI-MS analysis: Theoretical M^+: 550.0817 (100%); *found:* 550.0812 (100%). ^1H NMR ($(CD_3)_2CO$ δ / ppm): 8.99 (t, 2H); 8.87 (d, 1H); 8.77 (t, 2H); 8.64 (d, 1H); 8.28 (t, 2H); 8.00 (m, 2H); 7.92 (d, 1H); 7.88 (t, 1H); 7.80 (m, 2H); 7.67 (d, 1H); 7.60 (d, 1H); 7.36 (m, 3H); 7.12 (t, 1H); 4.20 (d, 1H); 4.04 (d, 1H).

The isolation of the oxidized complex, $[Ru(bpy)_2(acpyoxi)]PF_6$ was achieved by dissolving 0.300 g (0.43 mmol) of $[Ru(bpy)_2(acpy)]PF_6$ in 20 mL of acetone/H_2O (1:1). The solution was kept under oxygen atmosphere and stirring for 50 h at 298 K. Acetone was removed by evaporation under reduced pressure. The final product was collected as PF_6 salt by filtration with 90% yield. Single crystals of the $[Ru(bpy)_2(acpyoxi)]PF_6$ complex were obtained by dissolving $[Ru(bpy)_2(acpyoxi)]PF_6$ into a minimum amount of acetone. The solution was left in the dark for slow evaporation.

Calculated elemental analysis for $C_{27}H_{20}O_3N_5PF_6Ru.H_2O$ was C, 44.64%; N, 9.64%; H, 3.05%; *found:* C, 44.68%; N, 9.54%; H, 3.09%.^1H ($(CD_3)_2CO$ δ / ppm): 8.92 (d, 1H); 8.76 (d, 2H); 8.69 (t, 2H); 8.14 (m, 5H); 8.00 (m, 3H); 7.83 (m, 2H); 7.72 (d, 1H); 7.63 (t, 1H); 7,.7(t, 1H); 7.40 (dd, 2H). ESI-MS analysis: Theoretical M^+: 564.0609 (100%); *found:* 564.0610 (100%)

Experimental Techniques

Electronic absorption spectra were recorded on a double beam Shimadzu UV-1650 spectrophotometer. ^1H NMR spectra were recorded on a DRX-400 Bruker Ascend 400 MHz spectrometer at 298 K. Residual solvent signals or TMS were used as internal standards. Measurements were carried out in dry and argon aerated solvents to avoid contact with O_2. Attenuated total reflectance infrared (ATR-FTIR) spectra were recorded on a Perkin-Elmer Frontier spectrometer equipped with a diamond crystal plate, using 16 scans at a resolution of 4 cm^{-1}. Conductivity measurements were carried out in acetone

at 298 K employing a benchtop Tecnopon model mCA150 conductivity meter. A 10^{-3} mol L^{-1} $TBAPF_6$ solution was employed as standard 1:1 electrolyte (Λ_M = 157.0 μS cm^{-2} mol^{-1}).

Electrochemical measurements were carried out in a PGSTAT204 potentiostat (Metrohm Autolab) employing a glassy carbon working electrode, a platinum wire as the counterelectrode and Ag/AgCl (3 mol L^{-1} KCl) as the reference electrode. Potentials were corrected using ferrocene as the internal standard. 0.1 mol L^{-1} $TBAPF_6$ solutions in dichloromethane or in acetonitrile were employed as the supporting electrolyte. All potentials are presented *versus* Fc^+/Fc (E^o = 0.400 V vs SHE).

Single crystal X-ray diffraction was carried out in a Bruker APEX II Duo diffractometer. Data were acquired using a Mo-K_α radiation (λ = 0.71073 Å) and standard procedures were applied for data reduction and absorption correction. The structures were predicted by direct methods using SHELXS-97 and refined by using SHELXL2016 (G. M. Sheldrick, University of Göttingen, Göttingen, Germany, 2016). The positions of the hydrogen atoms were calculated in idealized positions and treated with the "riding model" option of the SHELXL2016 program. Non-hydrogen atoms were refined with anisotropic displacement parameters. Crystallographic data and experimental details of the structural analysis are summarized in Table S1.

Computational Methods

All geometries were fully optimized at the M06-L level of density functional theory[26] in conjunction SMD continuum solvation model[27] for dichloromethane using def2-TZVP basis set[28] on Ru and the def2-SVP basis set[28] on all other atoms. Non-analytical integrals were evaluated using the integral=grid=ultrafine option as implemented in the Gaussian 16 software package.[29] The nature of all stationary points was verified by analytic computation of vibrational frequencies, which were also used for the computation of zero-point vibrational energies, molecular partition functions, and for determining the reactants and products associated with each transition-state structure by following the normal modes associated with imaginary frequencies. Partition functions were used in the computation of 298 K thermal contributions to the free energy employing the usual ideal-gas, rigid-rotator,

harmonic oscillator approximation.[30] Free-energy contributions were added to single-point M06-L electronic energies computed using SMD continuum solvation model for dichloromethane at the optimized geometries obtained with the initial basis with the def2-TZVPP basis set on Ru and the def2-TZVP basis set on all other atoms to arrive at final, composite free energies. A 1 M standard state was used for all species in solution, thus, an adjustment for the 1 atm to 1 M standard-state concentration change of $RT\ln(24.5)$, (1.89 kcal/mol at 298 K) was added to the computed free energies.[30]

Time-dependent density functional theory (TDDFT) calculations were performed to predict the UV/visible electronic excitations of relevant structures. The B3LYP[31, 32] density functional, the def2-TZVPP basis set on Ru and the def2-TZVP basis set on all other atoms were used for the TDDFT calculations. Non-equilibrium solvation effects were included *via* the linear response approximations[33] in combination with the SMD continuum solvation model for dichloromethane.

Results

The new complex $[Ru(bpy)_2(acpy)]^+$ (acpy = 2-pyridylacetate, bpy = 2,2'-bipyridine) was successfully synthesized and its structure and electronic properties were compared with the parent $[Ru(bpy)_2(pic)]^+$ (pic = 2-pyridylcarboxylate) complex, which was first reported by Norrby et al.[24] Different from the picolinate, the acpy ligand in $[Ru(bpy)_2(acpy)]^+$ tends to labilize at room temperature in coordinating solvents, such as CH_3CN, so all spectroscopic and electrochemical measurements were carried out in anhydrous CH_2Cl_2 or acetone. Elemental analysis along with high resolution mass spectrometry and ^1H NMR spectroscopy have confirmed the purity of the synthesized products. Conductivity measurements carried out in 10^{-3} mol L^{-1} acetone solutions reveal that both complexes behave as 1:1 electrolyte (Λ_M = 154 and 158 μS cm^{-2} mol^{-1}, respectively for $[Ru(bpy)_2(pic)]PF_6$ and $[Ru(bpy)_2(acpy)]PF_6$).

^1H NMR spectra of both complexes are shown in Fig. S1 as well as H-H COSY data in Fig. S2 (Supplementary Information). It can be observed that the signals attributed to hydrogen atoms of the bpy ligands shift to higher frequencies upon coordination, whereas signals related to hydrogen atoms from pic and acpy ligands shift to lower frequencies as a result of the anisotropic

effect of the bipyridine ligands. Moreover, the hydrogen atoms from the additional CH_2 group in the acpy ligand become diastereotopic (^2J = 16.4 Hz) after coordination to the metal center.

UV-vis spectrum of $[Ru(bpy)_2(acpy)]^+$ is very similar to the parent $[Ru(bpy)_2(pic)]^+$ complex (Fig. 1). Low energy bands are ascribed to metal-to-ligand charge transfer ($MLCT_{Ru\rightarrow bpy}$) electronic transitions, while the high energy bands are related to intraligand (IL) transitions. TD-DFT calculations confirm such assignments and, additionally indicate some contribution of the metal to carboxylate-ligand charge transfer ($MLCT_{Ru\rightarrow pic}$ or $MLCT_{Ru\rightarrow acpy}$) to the high energy bands as clearly seen in the population of molecular orbitals of both complexes in the relevant electronic transitions (Table S1-S4). The occupied frontier molecular orbitals of both complexes exhibit dominant contribution from the *d* orbitals of the Ru^{II} center, while the lowest unoccupied molecular orbitals feature mostly π^* orbital character from the 2,2'-bipyridine ligand. The main calculated electronic transitions for the complexes and isosurface plots from the frontier orbitals are presented in Tables S2-S5.

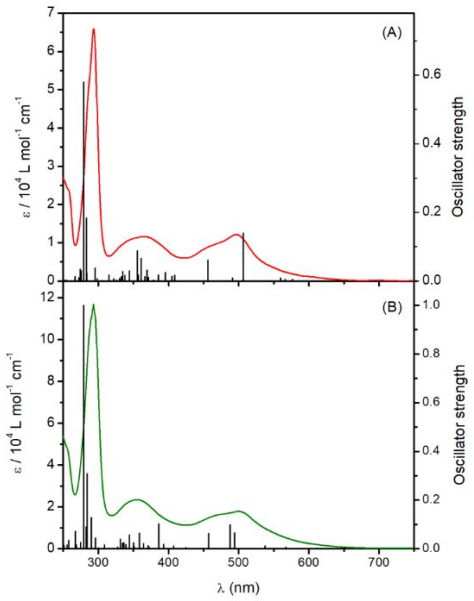

Figure 1. Experimental absorption spectra of (A) $[Ru(bpy)_2(pic)]^+$ and (B) $[Ru(bpy)_2(acpy)]^+$ in CH_2Cl_2. The bars refer to the oscillator strengths of TD-DFT calculated electronic transitions.

Distinct from the electronic spectra, the electrochemical properties of $[Ru(bpy)_2(acpy)]^+$ significantly differs from those of $[Ru(bpy)_2(pic)]^+$. As shown in Fig. 2, cyclic voltammograms (CV) of $[Ru(bpy)_2(pic)]^+$ obtained in acetonitrile

under argon are characterized by a reversible one electron redox process attributed to the Ru^{II}/Ru^{III} couple ($E_{1/2}$ = 0.88 vs Fc/Fc^+). On the other hand, the CVs of $[Ru(bpy)_2(acpy)]^+$ in dichloromethane exhibit three oxidative redox waves in the investigated electrochemical window. The first wave exhibits a reversible behavior and occurs at a lower potential than that observed for $[Ru(bpy)_2(pic)]^+$, being tentatively assigned to the Ru^{II}/Ru^{III} couple ($E_{1/2}$ = 0.55 vs Fc/Fc^+) based on the nature of the HOMO pointed by theoretical calculations. The further two oxidative processes occur at very close potentials overlapping with each other. Each peak can be clearly observed in the differential pulse voltammograms (Fig. S3). At fast scan rates the reductive peaks associated to the three processes can be observed, however at 10 mV s^{-1} the cathodic peak corresponding to the third oxidation process is not observed indicating the occurrence of a coupled chemical reaction (EC mechanism) following the electrochemical oxidation processes.

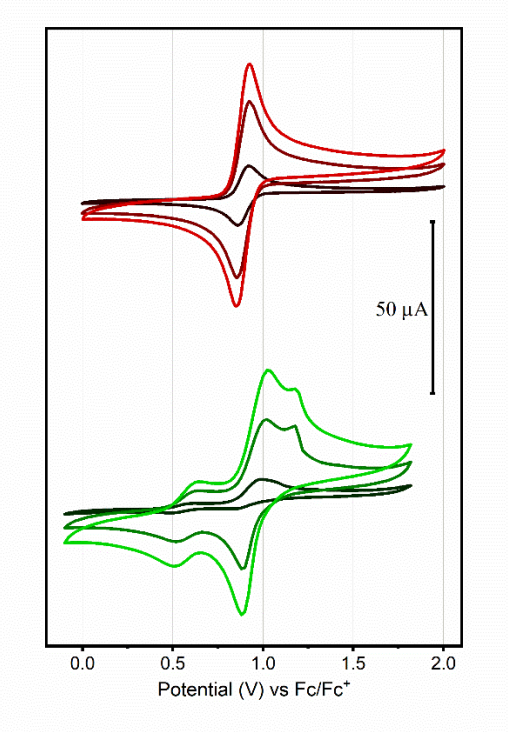

Figure 2. Cyclic voltammograms at 10, 100 and 200 mV s^{-1} of $[Ru(bpy)_2(pic)]^+$ (top) in acetonitrile and $[Ru(bpy)_2(acpy)]^+$ (bottom) in dichloromethane under argon. 0.1 mol L^{-1} $TBAPF_6$ was used as supporting electrolyte.

Based on the electrochemical behavior of the Hacpy ligand, which exhibits an irreversible oxidation wave at E = 1.53 V vs Fc/Fc^+ (Fig. S4), one

can tentatively attribute the second and third oxidation processes in $[Ru(bpy)_2(acpy)]^+$ respectively to the Ru^{III}/Ru^{IV} couple and to the one electron oxidation of the acpy ligand. Electrochemical data indicate that the substitution of 2-picolinate by 2-pyridylacetate leads to more negative potentials for the $Ru^{III/II}$ redox pair and also that the formation of Ru^{IV} becomes accessible, which apparently triggers the ligand oxidation. The free Hacpy ligand is irreversibly oxidized at a potential 500 mV higher than that observed for $[Ru(bpy)_2(acpy)]^+$. In fact, when the complex is exposed to the air in the dark, it undergoes slow and quantitative oxidation by O_2 yielding a coordinated α-oxo-2-pyridilacetate (acpyoxi) complex, Scheme 1, whose crystal structure is shown in Fig. 3. Additional characterization of the oxidation product is presented in Figures S5 (FTIR) and S6 (^{1}H NMR) in the supporting information. In the FTIR spectrum, new absorption bands can be observed at 1640 and 1649 cm^{-1}, typically observed for α-ketoesters. ^{1}H NMR reveal the disappearance of the methylene protons of the acpy ligand while the signals attributed to the protons in the pyridyl ring of the ligand are shifted to higher fields due to the presence of the carbonyl group. The oxidation product also behaves as 1:1 electrolyte in acetone (Λ_M = 135 μS cm^{-2} mol^{-1}).

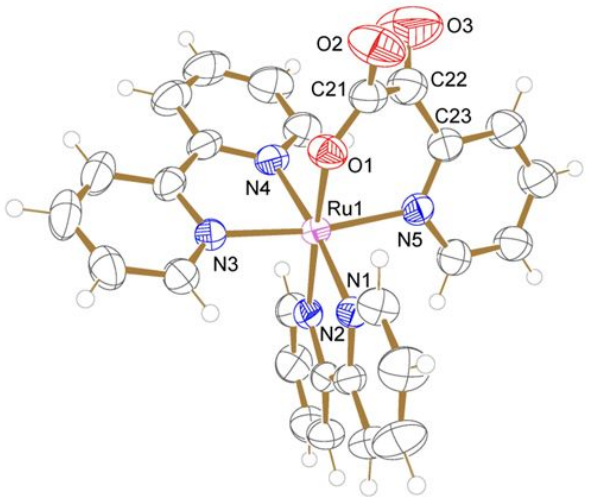

Ru1–O1	2.0854(19)
Ru1–N1	2.046(2)
Ru1–N2	2.043(2)
Ru1–N3	2.056(2)
Ru1–N4	2.067(2)
Ru1–N5	2.086(2)
C21–O1	1.257(4)
C21–O2	1.223(4)
C22–O3	1.215(5)
N2-Ru1-O1	170.79(9)
N1-Ru1-O1	91.92(9)
N3-Ru1-O1	84.21(8)
N3-Ru1-N5	170.65(9)
N1-Ru1-N4	173.67(9)

Figure 3. ORTEP representation of the $[Ru(bpy)_2(acpyoxi)]^+$ complex at 50 % probability level. PF_6^- anion was omitted for clarity. Selected bond lengths (Å) and angles (deg) are listed on the right. Full crystallographic data is presented at Table S5 of supporting information.

The product crystalizes in the monoclinic system, space group *C*2/*c* (Table S1), while the parental complex $[Ru(bpy)_2(pic)]PF_6$ (Table S5) crystalizes at monoclinic system with $P2_1/n$ space group. Attempts to crystalize the non-oxidized complex $[Ru(bpy)_2(acpy)]PF_6$ were not successful. The N(5)-Ru-O(1) angle in the complex with the oxidized ligand is 88.99º according to the diffraction data, a value very similar to that calculated at the M06-L level of theory for the coordinated acpy, but c.a. 10º higher than the one found for $[Ru(bpy)_2(pic)]PF_6$ (78.82º) [34]. Moreover, the Ru-N(5) distance in $[Ru(bpy)_2(acpyoxi)]PF_6$ is around 10% longer than that for $[Ru(bpy)_2(pic)]PF_6$ (2.086 Å) vs 2.060 Å).

Control experiments carried out in acetone and dichloromethane under inert atmosphere reveals that the initial complex $[Ru(bpy)_2(acpy)]^+$ remains unaltered, which indicates the role of molecular oxygen in the oxidation reaction. Isotope labeling experiments employing $^{18}O_2$ that could provide definitive experimental proof was unfortunately out of our capabilities. The reaction was probed under strictly dark conditions ruling out a photoinduced pathway. It is also worth noting that the formation of $[Ru(bpy)_2(acpyoxi)]^+$ occurs even at solid state as evidenced by ATR-FTIR, when the synthesized $[Ru(bpy)_2(acpy)]PF_6$ is left exposed to air for a long period of time. The oxidation of the α-C by O_2 to yield the diketone derivative does not occur for the free Hacpy ligand, which along with the electrochemical data indicate that the reaction should be mediated by the metal center, being one of the few examples of room temperature C-H activation by Ru complexes using O_2 as the primary oxygen donor.

As a next step, we investigated the kinetic and mechanistic aspects of the reaction between $[Ru(bpy)_2(acpy)]^+$ and molecular oxygen in detail by means of UV-Vis, MS and ^{1}H NMR measurements, along with theoretical calculations. Figures 4 and 5 show the UV-Vis and ^{1}H NMR spectral variations respectively, after solutions of $[Ru(bpy)_2(acpy)]^+$ in non-coordinated solvents were purged with O_2. The solubility of molecular oxygen in acetone and CH_2Cl_2 at 298 K and 101 kPa was assumed to be 1.2 x 10^{-2} and 1.1 x10^{-2} mol L^{-1} respectively.[35]

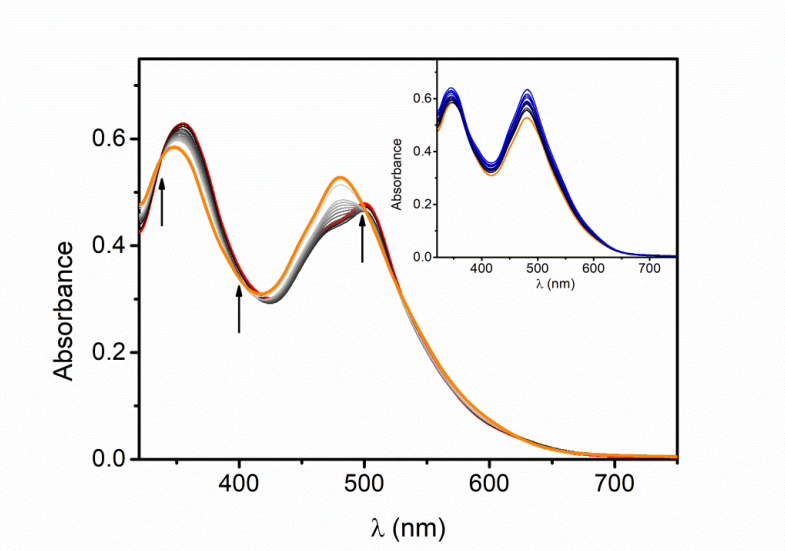

Figure 4. UV-vis spectral changes of $[Ru(bpy)_2(acpy)]^+$ in CH_2Cl_2 ($1.7x10^{-4}$ mol L^{-1}) before (red) and in the course (black to light gray) of the reaction with O_2 up to 23 hours (orange). *Inset*: Spectral changes from 23 (orange) to 100 h (black to blue). T = 298 K.

In the Figure 4, it can be observed that the initial absorption of the complex in the 450-500 nm region (red curve) slightly decreases after O_2 bubbling for five minutes. Then, for the next 23 hours, a blue shift at the lowest energy absorption maximum, from 500 to 480 nm, along with other spectral changes at higher energy were observed. At least three (pseudo)isosbestic points could be identified at 337, 404 and 501 nm. After 23 hours (orange curve), the (pseudo)isosbestic points were completely lost and the absorbance steadily increased for the next 100 hours after initial contact with O_2 (blue curves, Figure 4 – *inset*).

In the NMR spectra, more specifically in the region where the peaks from the diastereotopic hydrogen atoms of the CH_2 group in acpy appear, a downfield shift of the hydrogen signals in the first 15 hours is observed, Figure 5a. Concomitantly with the changes in the chemical shift, the relative areas of the peaks decreased as a function of the reaction time, indicating the oxidation of the CH_2 group. Additionally, the diastereotopic pattern was lost between 24 and 27 h after the contact with O_2, Figure 5b, which coincides with the disappearance of the (pseudo)isosbestic points in the UV-Vis spectrum. UV-Vis and NMR data together indicate the formation of at least, two reaction

intermediates. The first one seems to reach its maximum concentration within the initial 15 h of reaction, while the concentration of the second one increases between 15 and 27 h and then it is further oxidized to the final product.

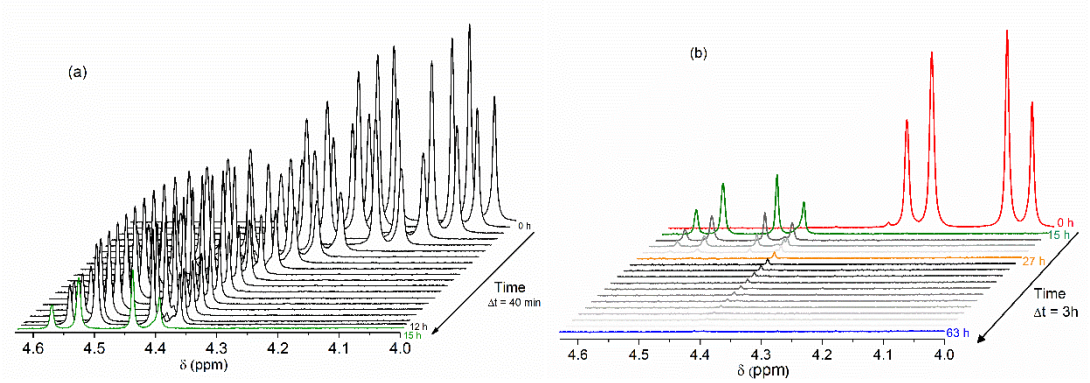

Figure 5. ^{1}H NMR spectral changes of $[Ru(bpy)_2(acpy)]^+$ solutions ($2.1x10^{-3}$ mol L^{-1}) as a function of time after purging the solution with O_2. In (a) spectra for first 12 hours (Δt = 40 min) and after 15 hous (green) are shown, while in (b) data from 15 to 63 hours (Δt = 3 hours) are compared to the starting spectrum. CD_6CO (298 K); 400 MHz.

Further information about the nature of the reaction intermediates can be obtained from the aromatic region in ^{1}H NMR spectrum (Figure 6). As the oxidation proceeded, shifts in the original peaks as well as the appearance of new signals were observed. Particularly, a peak at low field (10.56 ppm) appeared in the first hours of reaction and reached its maximum intensity around 15 h after the reaction started. We tentatively assigned this broad peak to the hydrogen atom of the hydroxy group, which is deshielded due to the hydrogen bonding interaction with the carboxylic group, Scheme 2.

In Figure 6, a peak at c.a. 9.14 ppm appeared as the reaction took course. Its relative area increased steadily in the first 8 hours and then decreased as the signal at 10.56 ppm increased, indicating that the formation of the α-hydroxo carboxylate species occurs through another intermediate. Both peaks were not present at all after 60 h. At this point the ^{1}H NMR spectrum resembled that obtained for the final product, $[Ru(bpy)_2(acpyoxi)]^+$ (Fig. S6).

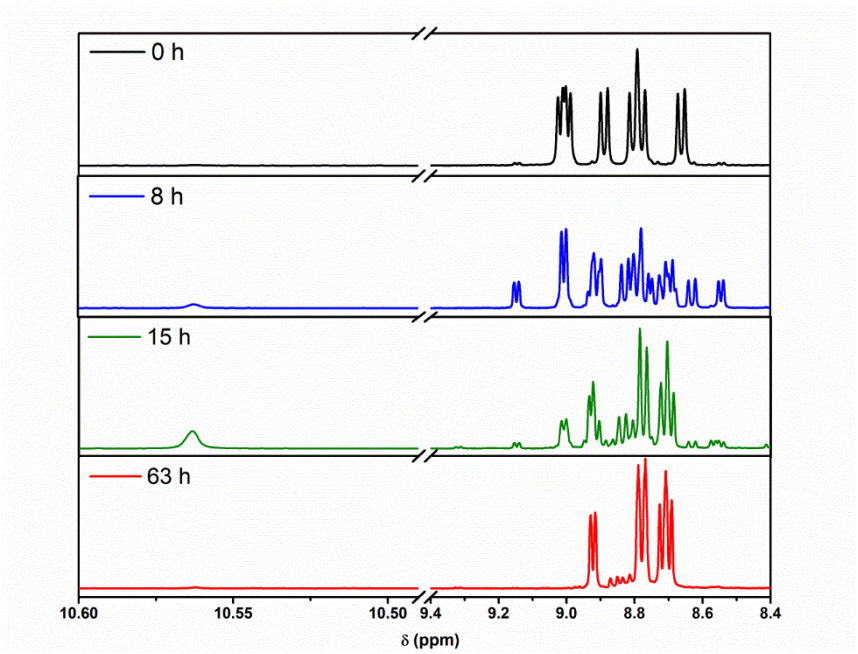

Figure 6. ^{1}H NMR spectral changes in the aromatic region of $[Ru(bpy)_2(acpy)]^+$ solutions ($2.1x10^{-3}$ mol L^{-1}) in selected reaction times after contact with O_2. CD_6CO (298 K); 400 MHz

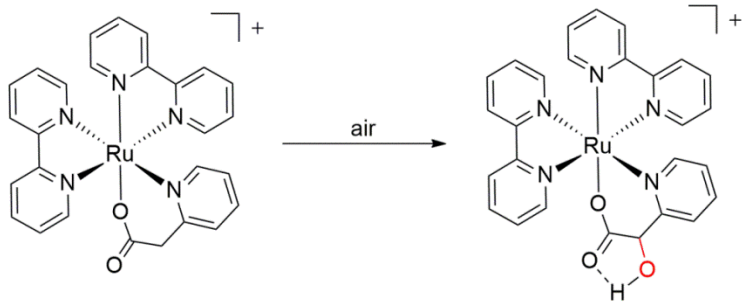

Scheme 2. Formation of the coordinated α-hydroxo carboxylate species

Kinetic analysis was performed considering a pseudo-first order model in relation to the metal complex concentration. For UV-Vis data, analysis was carried out employing the absorption changes at 481 nm. For ^{1}H NMR data, TMS was employed as internal standard, allowing to quantitatively correlate the decrease of the area relative to the hydrogen atoms in the CH_2 group of the coordinated acpy ligand in a given reaction time due to the oxidation process. In both cases, good linearity could be observed up to 15 h after the reaction started (Fig. S7), corresponding to the formation of the first oxidation product, $[Ru^{II}(bpy)_2(\alpha\text{-OH-acpy})]^+$. The observed rate constant (k_{obs}) determined by UV-

Vis was (9.2 ± 0.2) x 10^{-2} h^{-1}, Fig. S7(A) and a similar value, (8.7 ± 0.3) x 10^{-2} h^{-1}, was found using ^{1}H NMR data, Fig. S7(B).

The reaction was also followed by mass spectrometry (Fig. S8). For that, a fresh solution of $[Ru(bpy)_2(acpy)]^+$ was prepared under inert and dark conditions. The solution was then bubbled with O_2 and aliquots were analyzed within the first hour after contact with O_2. The data reveal that the initial complex (M^+ = 550.0829) quickly reacted with molecular O_2 to yield an intermediate of M^+ = 566.0757 (Fig. S8), meaning the addition of one oxygen atom to the initial complex. Taking the ^{1}H NMR data discussed above, this peak can be tentatively associated to the complex with the α-hydroxo carboxylate ligand (Scheme 2), although other plausible structures such as the Ru^{IV}=O complex $[Ru^{IV}(bpy)_2(acpy)O]^+$ could be also proposed. The mass spectra also reveal the formation of a species with M^+ = 582.0734, which means the addition of two oxygen atoms to the initial complex. Given the role of molecular oxygen on triggering the reaction and the direct rule of the metal center in the reaction, this molecular ion peak is tentatively attributed to an intermediate formed by the initial O_2 coordination to the Ru center to generate a Ru^{III}-$OO^{\bullet-}$ complex, Scheme 3. The experimental data do not allow a definitive assignment but as it will be discussed below, theoretical calculations corroborate with the proposed structure.

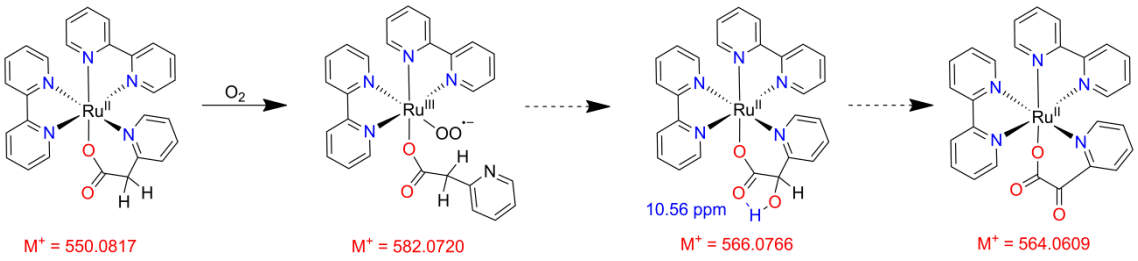

Scheme 3. Proposed reaction intermediates for the oxidation of the coordinated 2-pyridylacetate to α-oxo-2-pyridylacete by molecular oxygen.

The experimental data so far suggests that the oxidation of the coordinated 2-pyridylacetate ligand is mediated by the ruthenium center and involves molecular oxygen. The reaction may follow inner or outer sphere mechanisms and the available experimental data do not allow to exclude any of these possibilities. For inner sphere mechanism, coordination of O_2 to the Ru

center followed by intramolecular C-H activation or formation of 7-coordinated species can be considered. Alternatively, an outer sphere electron transfer reaction between $[Ru(bpy)_2(acpy)]^+$ and molecular O_2[36-39] would be also a possibility. In the following, we employed density functional theory (DFT) calculations at the M06-L level in conjunction with SMD continuum model for dichloromethane to evaluate the thermodynamics and kinetics of the most plausible reaction pathways in detail.

(a) Inner sphere mechanism. We started our investigation by computing the initial O_2 coordination to generate Ru^{III}-$OO^{\bullet-}$ intermediate for both $[Ru(bpy)_2(acpy)]^+$ and $[Ru(bpy)_2(Hacpy)]^{2+}$ complexes. Since there's no experimental evidence for the generation of protonated form of the complex, $[Ru(bpy)_2(Hacpy)]^{2+}$, here we will focus on $[Ru(bpy)_2(acpy)]^+$ and the results for the former are presented in the supporting information, Fig. S9 and Scheme S1. For the oxygen binding step, possible decoordination of both pyridyl N and acetate O atoms were considered, Figure 7, with the former being favored by about 15 kcal mol^{-1} (ΔG = 17.6 vs ΔG = 32.7 kcal mol^{-1} respectively). This is in line with the Ru^{III} oxidation state character of the superoxo complex, as Ru^{III} center will favor the coordination of harder bases like the O atom of the carboxylate anion ($[Ru^{III}(bpy)_2(\textit{O-acpy})O_2]^+$) over the pyridine N atom ($[Ru^{III}(bpy)_2(\textit{N-acpy})O_2]^+$) as has been shown in earlier studies.[40]

The initial coordination of O_2 in $[Ru(bpy)_2(acpy)]^+$ seems to be favored by the relatively low stability of the six-membered ring chelate formed by the acpy ligand in comparison with five-membered ring chelates such as that formed in $[Ru(bpy)_2(pic)]^+$. In fact, the acpy ligand is more labile than its picoline counterpart in coordinating solvents such as acetonitrile in line with the computed free energy changes for acetonitrile coordination to be favored by 3 kcal/mol for $[Ru(bpy)_2(acpy)]^+$ (ΔG = 17.6 kcal/mol) compared to that of $[Ru(bpy)_2(pic)]^+$ (ΔG = 22.8 kcal/mol). Moreover, the observed rate constant for the solvolysis of the acpy ligand in $[Ru(bpy)_2(acpy)]^+$ in acetonitrile is $2.5x10^{-1}$ h^{-1} at 298 K (Figure S10), 10 times higher than the ligand oxidation which could explain why oxidation reaction is not observed in this solvent. The same behavior is observed if small amounts of OH^- or triethylamine is added to the

system, i.e. the acpy is partially or fully labilized, Fig. S11, hindering the C-H activation.

As Ru(II) exhibits high affinity to pyridyl ligands, the nucleophilic attack by O_2 could occur by initial detachment of the coordinated carboxylate group to yield the Ru^{III}-$OO^{\bullet-}$ center. As Ru(III) is formed, the affinity to the carboxylate group increases and isomerization yields the more stable $[Ru^{III}(bpy)_2(O\text{-}acpy)O_2]^+$ intermediate, Scheme 4.

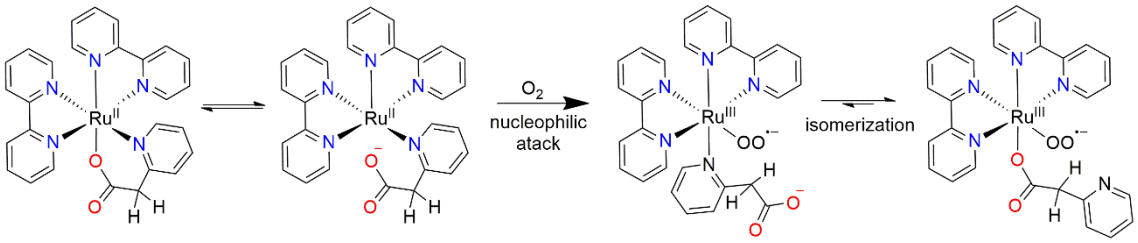

Scheme 4. Proposed reaction pathway for the formation of the $[Ru^{III}(bpy)_2(O\text{-}acpy)O_2]^+$ intermediate by nucleophilic attack of O_2 in the $[Ru(bpy)_2(acpy)]^+$ complex.

An alternative to the pathway shown in the Scheme 4 would be the formation of a 7-coordinated species as previously shown by Kojima et al [41]. In fact, we have shown the feasibility of seven coordination for formally Ru(IV)=O and Ru(V)=O species for water oxidation catalysts in our recent studies[42-44] but the current ligand framework is not suitable for seven coordination around the Ru center. Efforts for optimizing seven-coordinated geometries led to formation of six coordinate Ru species.

We then considered the C-H bond activation by Ru^{III}-$OO^{\bullet-}$ and the located transition states feature $\Delta G^{\ddagger}$ of 23.5 and 20.5 kcal mol^{-1} for $[Ru^{III}(bpy)_2(O\text{-}acpy)O_2]^+$ and $[Ru^{III}(bpy)_2(N\text{-}acpy)O_2]^+$ respectively (Figure 7). Taking into account the free energy cost for the initial oxygen binding step, the overall free energy of C-H bond activation are 41.1 and 53.2 kcal mol^{-1} for $[Ru^{III}(bpy)_2(O\text{-}acpy)O_2]^+$ and $[Ru^{III}(bpy)_2(N\text{-}acpy)O_2]^+$ isomers respectively, which renders this pathway to be quite unlikely.

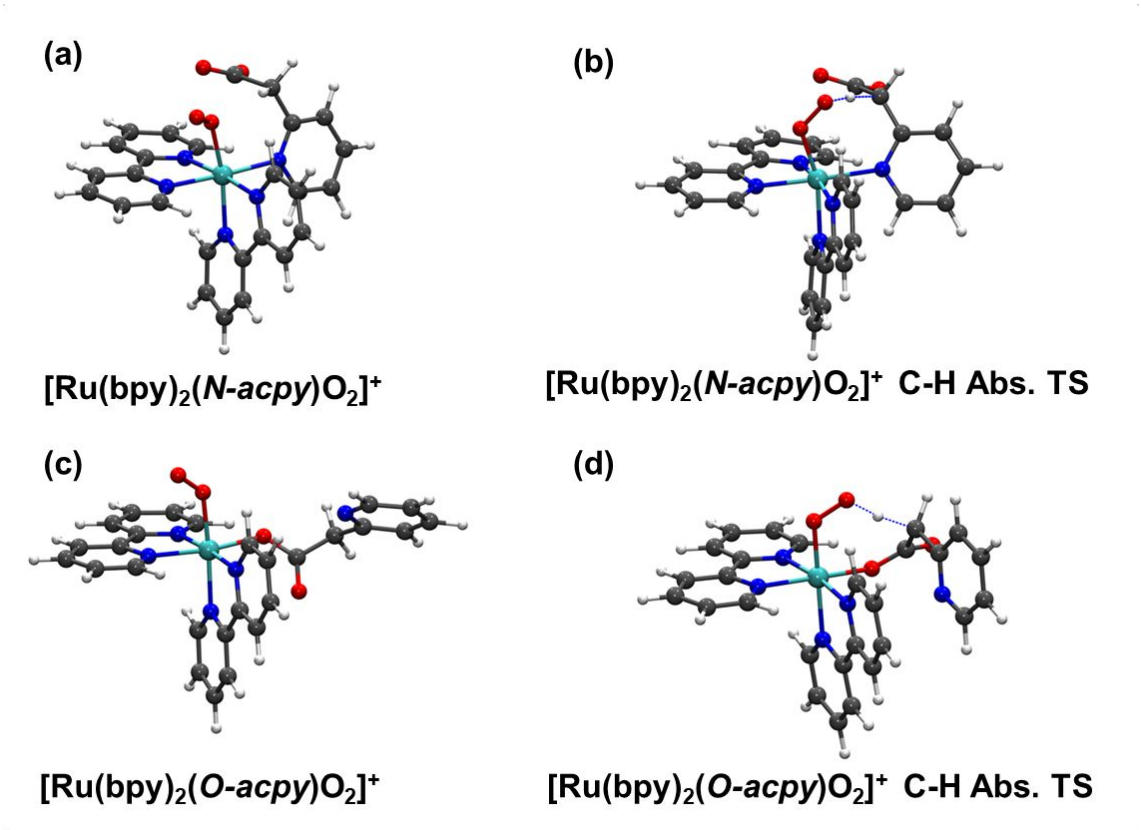

Figure 7. Optimized structures of **(a)** $[Ru(bpy)_2(N\text{-}acpy)O_2]^+$, **(c)** $[Ru(bpy)_2(O\text{-}acpy)O_2]^+$ and **(b** and **d)** associated transition states for C-H abstraction. Color code: Ru, cyan; C, gray; O, red; N blue and H white.

Next, we turned our attention to the possible reaction of $[Ru^{III}(bpy)_2(O\text{-}acpy)O_2]^+$ with another $[Ru^{II}(bpy)_2(acpy)]^+$ complex to generate a diruthenium μ-peroxo intermediate, $[(Ru^{III}(bpy)_2(O\text{-}acpy))_2O_2]^{2+}$ (Figure 8a) and found it to be quite feasible with a ΔG of −2.1 kcal mol^{-1} (Scheme 4). The ground state for $[(Ru^{III}(bpy)_2(O\text{-}acpy))_2O_2]^{2+}$ is a singlet with antiferromagnetically coupled Ru centers (Fig. S12a) whereas a triplet structure with ferromagnetic coupling of the two metal centers lies within 4.7 kcal/mol (Fig. S12b). Interestingly, the cleavage of the O-O bond in $[(Ru^{III}(bpy)_2(O\text{-}acpy))_2O_2]^{2+}$ (Figure 8b) to generate two $[Ru^{IV}(bpy)_2(O\text{-}acpy)O]^+$ (Figure 8c) proceeds with a low activation free energy ($\Delta G^{\ddagger}$) of 2.3 kcal mol^{-1}. The intermediacy of Ru(IV) center was suggested by Diamond et al. for the oxidation of coordinated primary and secondary amines[45] and also by Pladziewicz et. al. for the O_2 reduction by $[Ru^{II}(NH_3)_6]^{2+}$ into H_2O_2.[46] A similar mechanism was also proposed by Tovrog et al.[47] for the oxidation of 2-1'-hydroxyethylpyridine coordinated to $[Ru^{II}(NH_3)_4]^{2+}$

moiety by molecular oxygen to yield H_2O_2 and the corresponding Ru^{II}-ketone complex. More recently, Ray and coworkers[14] reported catalytic alcohol oxidation by O_2 employing a Ru^{II}-hydride complex as the catalyst in which the reaction mechanism also involves the formation of Ru^{IV}=O species. Other examples can be found employing strong oxidants in water or other oxo donors.[41] However, no information is available for the initial step of the oxidation process, i.e. the O_2 activation by the Ru^{II} complexes. This information is vital for the development of potential oxidation catalysts which could use O_2 as the primary oxidant and a potential pathway could involve a dimer intermediate as proposed above.

As a next step, the Ru^{IV}=O (or Ru^{III}-$O^{\bullet-}$) center in $[Ru^{IV}(bpy)_2(O\text{-}acpy)O]^+$ complex can promote the C-H activation of the CH_2 group in the acpy ligand (Figure 8d) with a $\Delta G^{\ddagger}$ of 23.1 kcal/mol resulting in the formation of a Ru^{III}-OH complex with a carbon based radical (ΔG = 12.7 kcal mol^{-1}), $[Ru^{III}(bpy)_2(O\text{-}acpy^{\bullet})OH]^+$ (Figure 8e). Then, the hydroxo group is transferred to the α-C radical through a nearly barrierless process and could create *R* and *S* enantiomers of α-hydroxy-2-pyridylacetate. The energetics for the following steps will be presented only for *(S)*-α-hydroxy-2-pyridylacetate and those for *(R)* structure are presented in supporting information (Scheme S2-S3). The formation of $[Ru^{II}(bpy)_2(\alpha\text{-OH-acpy})]^+$ (Fig. 8f) (the *S* notation is dropped for brevity) from $[Ru^{III}(bpy)_2(O\text{-}acpy^{\bullet})OH]^+$ intermediate is computed to be very favorable (ΔG = –31.3 kcal mol^{-1}) (Scheme 5).

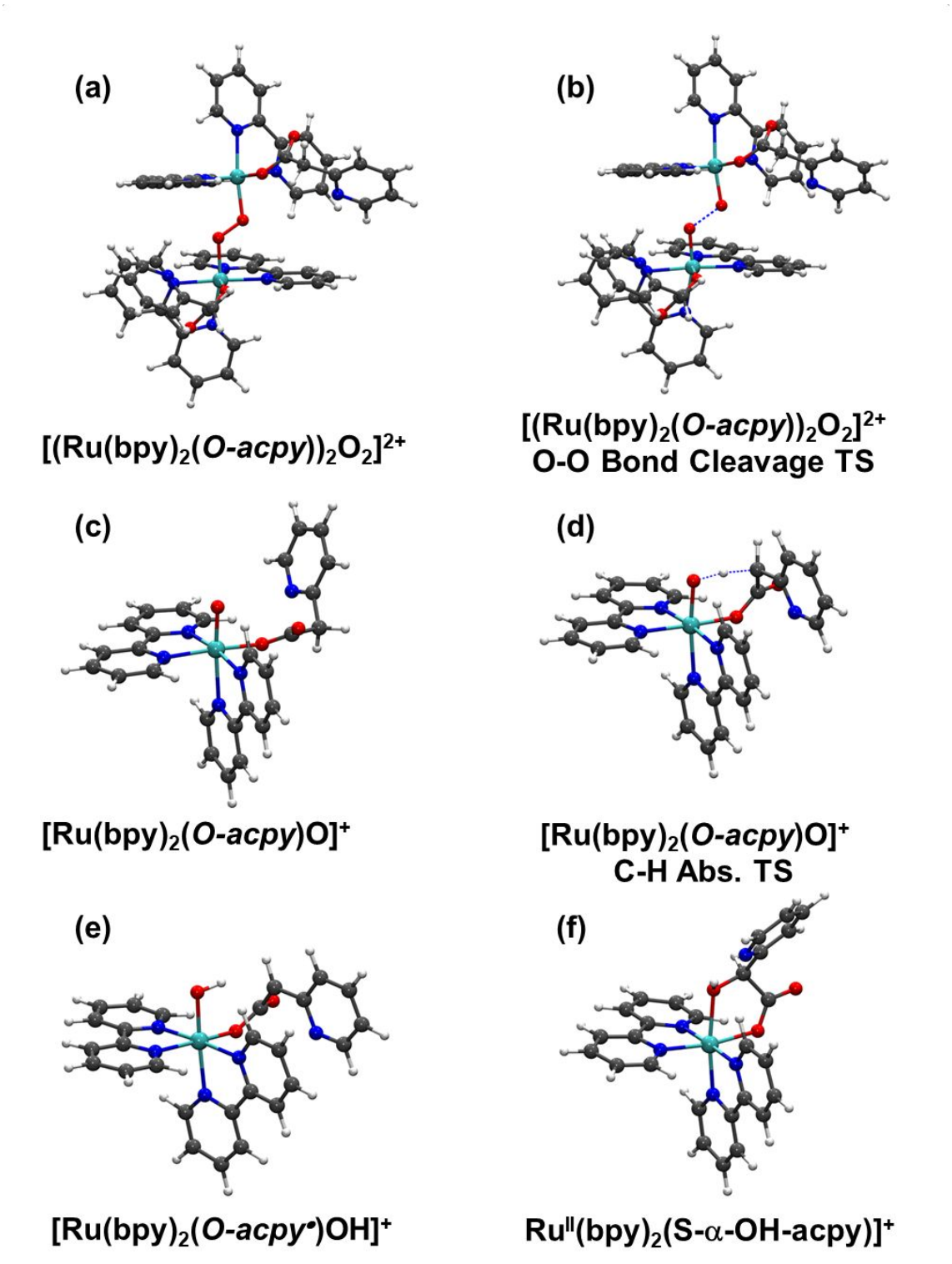

Figure 8. Optimized structures of **(a)** $[(Ru(bpy)_2(O\text{-}acpy))_2O_2]^{2+}$, **(b)** $[(Ru(bpy)_2(O\text{-}acpy))_2O_2]^{2+}$ O-O Bond Cleavage TS, **(c)** $[Ru(bpy)_2(O\text{-}acpy)O]^{+}$, **(d)** $[Ru(bpy)_2(O\text{-}acpy)O]^{+}$ C-H abstraction TS, **(e)** $[Ru(bpy)_2(O\text{-}acpy\text{-}C^{\bullet})OH]^{+}$ and **(f)** $[Ru^{II}(bpy)_2(S\text{-}\alpha\text{-}OH\text{-}acpy)]^{+}$. Color code: Ru, cyan; C, gray; O, red; N blue and H white.

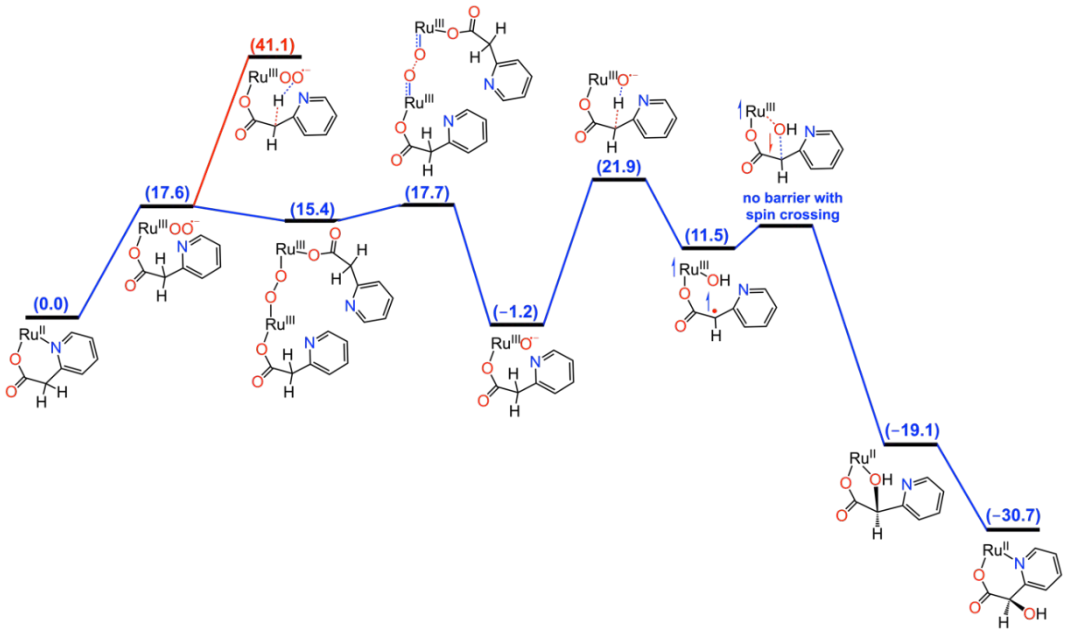

Scheme 5. Free energy profile of proposed mechanism of the O_2 reduction by $[Ru(bpy)_2(acpy)]^{2+}$ and C-H activation to yield the $[Ru^{II}(bpy)_2(S\text{-}\alpha\text{-}OH\text{-}acpy)]^{+}$. Bpy groups are omitted for clarity.

We further investigated the oxygen binding, diruthenium μ-peroxo formation and generation of reactive $[Ru^{IV}(bpy)_2(O\text{-}\alpha\text{-}OH\text{-}acpy)O]^{+}$ species from the $[Ru^{II}(bpy)_2(\alpha\text{-}OH\text{-}acpy)]^{+}$ complex and found similar energetics for both *R* (Scheme S3) and *S* (Scheme S4) stereoisomers of α-hydroxy-2-pyridylacetate to the parent $[Ru^{II}(bpy)_2(acpy)]^{+}$ system. Starting from $[Ru^{IV}(bpy)_2(O\text{-}\alpha\text{-}OH\text{-}acpy)O]^{+}$ C-H activation to generate $[Ru^{III}(bpy)_2(O\text{-}\alpha\text{-}OH\ \text{-}acpy^{\bullet})OH]^{+}$ was computed to proceed with a $\Delta G^{\ddagger}$ of 20.7 kcal/mol (Scheme 6). Upon formation of $[Ru^{III}(bpy)_2(O\text{-}\alpha\text{-}OH\ \text{-}acpy^{\bullet})OH]^{+}$, two possible pathways could be followed to generate the $[Ru(bpy)_2(O\text{-}acpyoxi)(OH_2)]^{+}$ intermediate (Scheme 6). The first one starts with a proton transfer step featuring low activation free energies for both triplet ($\Delta G^{\ddagger}$ = 6.9 kcal/mol) and open-shell singlet ($\Delta G^{\ddagger}$ = 2.1 kcal/mol) transition state structures leading to closed-shell ground-state $[Ru^{II}(bpy)_2(Hacpy)OH]^{+}$ (ΔG = −2.6 kcal/mol) species which upon further proton transfer forms $[Ru(bpy)_2(O\text{-}acpyoxi)(OH_2)]^{+}$. The other pathway involves a concerted electron proton electron transfer (EPT) step where α-OH proton is transferred to hydroxyl group coordinated to metal center with concomitant

electron transfer from carbon based radical to Ru^{III} center resulting in a common $[Ru(bpy)_2(O\text{-}acpyoxi)(OH_2)]^+$ intermediate (ΔG = –21.6 kcal/mol). The evolution of H_2O together with coordination of pyridine N atom to Ru center is quite favorable (ΔG = –16.5 kcal/mol) generating the final $[Ru(bpy)_2(acpyoxi)]^+$ product (Scheme 6). It should also be noted that the oxidation of the $[Ru^{II}(bpy)_2(\alpha\text{-}OH\text{-}acpy)]^+$ intermediate could also involve an *outer sphere mechanism* different than $[Ru^{II}(bpy)_2(acpy)]^+$.

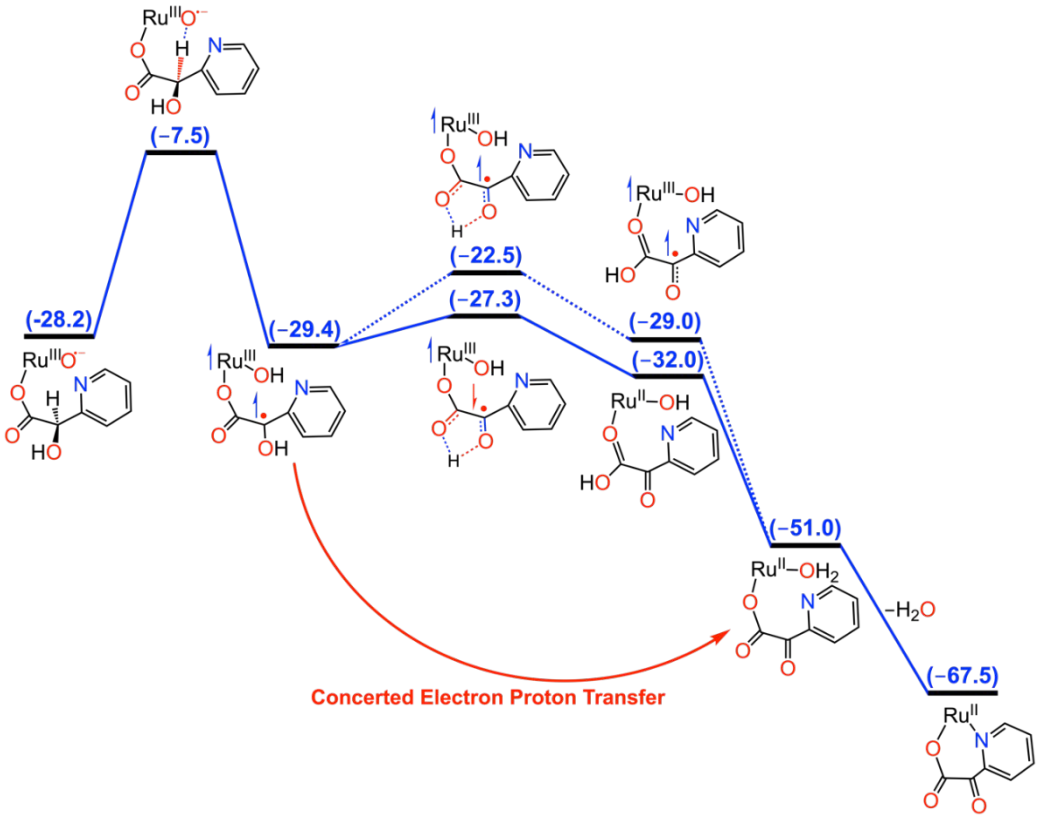

Scheme 6. Free energy profile of proposed mechanism of the C-H activation by $[Ru^{IV}(bpy)_2(O\text{-}\alpha\text{-}OH\text{-}acpy)O]^+$ to yield the $[Ru(bpy)_2(acpyoxi)]^+$. Bpy groups are omitted for clarity.

The theoretical calculations corroborate with the experimental data indicating that the highest activation energy for both the formation of the α-OH-acpy intermediate and the final product (Scheme 5 and 6, respectively) is related to the C-H activation step and should lead to a pseudo-first order kinetic behavior as observed. The consumption of the paramagnetic species is also found to be nearly barrierless, which explains the lack of observation of any influence of such species on the ^1H NMR data. Our attempts to identify

spectroscopic signatures of the proposed Ru(IV)=O species by Raman spectroscopy at room temperature were unsuccessful.

We should also note that in the proposed mechanism the O_2 cleavage to yield Ru^{IV}=O through the formation of a μ-peroxo bridge between two Ru^{II} centers resembles the pathway proposed by Nguyen et al[48] for a square planar Co^{II} complex and can be seen as the reverse process of O_2 evolution from water by Ru^{II}-OH_2 molecular catalysts through the so-called oxo-oxo coupling (I2M mechanism), despite in this case Ru^{V}=O species are involved.[19] In $[Ru(bpy)_2(acpy)]^{2+}$, as in the $[Ru^{II}(bda)(L)_2]$ water oxidation catalysts [49, 50], the carboxylate groups play a key role in stabilizing high oxidation states of the metal center (Ru^{IV}=O or Ru^{V}=O). Particularly, in the complex with the acpy ligand, the initial lability of the carboxylate group favors the nucleophilic attack by O_2 and, following the formation of Ru^{III}-$OO^{\bullet-}$, the carboxylate group replaces the pyridine in the coordination sphere, stabilizing the oxidized metal center. More importantly, this strategy can be conveniently employed to C-H bond activation using O_2 as the primary oxidant.

(b) Outer sphere mechanism. C-H activation via an outer sphere single electron transfer (SET) reaction involving the starting complex $[Ru(bpy)_2(acpy)]^{+}$ and O_2 was also computed, followed by hydrogen abstraction to yield a carbon based radical and hydroperoxyl radical, Figure S13. However, the closer inspection of the electronic structure of these species indicate that electron transfer (ET) to O_2 does not really occur and an charge transfer between carbon based radical and Ru(II) is observed. The located transition state for the hydrogen abstraction by O_2 features a $\Delta G^{\ddagger}$ of 38.6 kcal/mol and the overall ΔG for the reaction is 37.9 kcal/mol. These values are considerably higher than those found for the C-H activation by the above proposed inner sphere mechanism, which points out that the latter is likely the main reaction pathway although possible superoxide anion radical ($O_2^{\bullet-}$) formation by SET as reactive species cannot be completely ruled out.

Conclusions

The six-ring chelate formed by the coordination of the acpy ligand in $[Ru(bpy)_2(acpy)]^{+}$ is thermodynamically more unstable than the corresponding

five-ring chelate in $[Ru(bpy)_2(pic)]^+$. In the absence of coordinating solvents and under aerobic conditions, such instability of $[Ru(bpy)_2(acpy)]^+$ favors the nucleophilic attack of O_2 molecules to Ru^{II} centers to yield Ru^{III}-$OO^{\bullet-}$ superoxyl species that are promptly stabilized by the presence of a carboxylate group in the coordination sphere. Theoretical calculations indicate the formation of Ru^{IV}=O centers through a μ-peroxo intermediate formed by the reaction between Ru^{III}-$OO^{\bullet-}$ and a second $[Ru(bpy)_2(acpy)]^+$ complex. The resulting Ru^{IV}=O (or Ru^{III}-$O^{\bullet-}$) species triggers the C-H activation of the methylene group in the acpy ligand to yield, firstly the α-hydroxo carboxylate intermediate and then the corresponding α-keto carboxylate ligand. Surprisingly, the formation of Ru^{IV} centers from the reaction of $[Ru(bpy)_2(acpy)]^+$ and O_2 requires relatively low energetic input, which calls attention to the potential use of this strategy for catalytic oxidations of organic compounds using O_2 as the primary oxidant. Future efforts will target the use of the oxidation product $[Ru(bpy)_2(acpyoxi)]^+$ as a catalyst for aerobic dehydrogenation reactions.

Acknowledgments

This work was supported by Fundação de Amparo à Pesquisa do Estado de Minas Gerais (FAPEMIG, PPM-00220-17), Conselho Nacional de Desenvolvimento Científico e Tecnológico (CNPq, 406392/2018-8 and 305432/2017-6) and Coordenação de Aperfeiçoamento de Pessoal de Nível Superior (CAPES). The authors are also thankful to the Grupo de Materiais Inorgânicos do Triângulo (GMIT), a research group supported by FAPEMIG (APQ-00330-14). A.O.T.P. is thankful to Alexander Von Humboldt Foundation for the financial support. The work at Brookhaven National Laboratory (M.Z.E and J.J.C.) was carried out under contract DE-SC0012704 with the U.S. Department of Energy, Office of Science, Office of Basic Energy Sciences.

References

1. R. Ray, A. S. Hazari, G. K. Lahiri and D. Maiti, *Chem. Asian J.*, 2018, **13**, 2138-2148.
2. B. Karimi, O. Yari, M. Khorasani, H. Vali and F. Mansouri, *Chemcatchem*, 2018, **10**, 1783-1787.
3. J. Chen, S. Stepanovic, A. Draksharapu, M. Gruden and W. R. Browne, *Angew. Chem. -Int. Ed.*, 2018, **57**, 3207-3211.

4. Z. N. Lv, H. B. Wang, Z. Q. Chen, S. H. Zou, S. S. Zhu, C. L. Lou and G. C. Yin, *Mol. Cat.*, 2017, **432**, 259-266.
5. C. W. Anson, S. Ghosh, S. Hammes-Schiffer and S. S. Stahl, *J. Am. Chem. Soc.*, 2016, **138**, 4186-4193.
6. M. S. Sigman and D. R. Jensen, *Acc. Chem. Res.*, 2006, **39**, 221-229.
7. D. R. Jensen, M. J. Schultz, J. A. Mueller and M. S. Sigman, *Angew. Chem. Int. Ed.*, 2003, **42**, 3810-3813.
8. B. L. Ryland and S. S. Stahl, *Angew. Chem. Int. Ed.*, 2014, **53**, 8824-8838.
9. J. M. Hoover and S. S. Stahl, *J. Am. Chem. Soc.*, 2011, **133**, 16901-16910.
10. M. F. Semmelhack, C. R. Schmid, D. A. Cortes and C. S. Chou, *J. Am. Chem. Soc.*, 1984, **106**, 3374-3376.
11. R. Lingayya, M. Vellakkaran, K. Nagaiah and J. B. Nanubolu, *Asian J. Org. Chem.*, 2015, **4**, 462-469.
12. M. M. Tamizh, K. Mereiter, K. Kirchner and R. Karvembu, *J. Org. Chem.*, 2012, **700**, 194-201.
13. A. Taketoshi, X. N. Beh, J. Kuwabara, T. Koizumi and T. Kanbara, *Tetrahedron Lett.*, 2012, **53**, 3573-3576.
14. R. Ray, S. Chandra, D. Maiti and G. K. Lahiri, *Chem. Eur. J.*, 2016, **22**, 8814-8822.
15. Z. Lv, H. Wang, Z. Chen, S. Zou, S. Zhu, C. Lou and G. Yin, *Mol. Cat.*, 2017, **432**, 259-266.
16. A. Taketoshi, A. Tsujimoto, S. Maeda, T. Koizumi and T. Kanbara, *ChemCatChem*, 2010, **2**, 58-60.
17. T.-a. Koizumi and T. Kanbara, *Bull. Japan Soc. Coord. Chem.*, 2010, **56**, 14-23.
18. B. A. Moyer and T. J. Meyer, *J. Am. Chem. Soc.*, 1978, **100**, 3601-3603.
19. S. {Norrby, David W., Y. Xie and J. J. Concepcion, *Chem. Soc. Rev.*, 2017, **46**, 6170-6193.
20. S. F. Sousa and A. O. T. Patrocinio, *Quim. Nova*, 2014, **37**, 886-895.
21. W. J. Song, Z. F. Chen, M. K. Brennaman, J. J. Concepcion, A. O. T. Patrocinio, N. Y. M. Iha and T. J. Meyer, *Pure Appl. Chem.*, 2011, **83**, 749-768.
22. J. J. Concepcion, J. W. Jurss, M. K. Brennaman, P. G. Hoertz, A. O. T. Patrocinio, N. Y. M. Iha, J. L. Templeton and T. J. Meyer, *Acc. Chem. Res.*, 2009, **42**, 1954-1965.
23. R. Matheu, P. Garrido-Barros, M. Gil-Sepulcre, M. Z. Ertem, X. Sala, C. Gimbert-Suriñach and A. Llobet, *Nat. Rev. Chem.*, 2019, **3**, 331-341.
24. T. Norrby, A. Börje, B. Åkermark, L. Hammarström, J. Alsins, K. Lashgari, R. Norrestam, J. Mårtensson and G. Stenhagen, *Inorg. Chem.*, 1997, **36**, 5850-5858.
25. B. P. Sullivan, D. J. Salmon and T. J. Meyer, *Inorg. Chem.*, 1978, **17**, 3334-3341.
26. Y. Zhao and D. G. Truhlar, *J. Chem. Phys.*, 2006, **125**, 194101.
27. A. V. Marenich, C. J. Cramer and D. G. Truhlar, *J. Phys. Chem. B*, 2009, **113**, 6378-6396.
28. F. Weigend and R. Ahlrichs, *Phys. Chem. Chem. Phys.*, 2005, **7**, 3297-3305.
29. M. J. T. Frisch, G. W.; Schlegel, H. B.; Scuseria, G. E.; Robb, M. A.; Cheeseman, J. R.; Scalmani, G.; Barone, V.; Petersson, G. A.; Nakatsuji, H.; Li, X.; Caricato, M.; Marenich, A. V.; Bloino, J.; Janesko, B. G.; Gomperts, R.; Mennucci, B.; Hratchian, H. P.; Ortiz, J. V.; Izmaylov, A. F.; Sonnenberg, J. L.; Williams-Young, D.; Ding, F.; Lipparini, F.; Egidi, F.; Goings, J.; Peng, B.; Petrone, A.; Henderson,

T.; Ranasinghe, D.; Zakrzewski, V. G.; Gao, J.; Rega, N.; Zheng, G.; Liang, W.; Hada, M.; Ehara, M.; Toyota, K.; Fukuda, R.; Hasegawa, J.; Ishida, M.; Nakajima, T.; Honda, Y.; Kitao, O.; Nakai, H.; Vreven, T.; Throssell, K.; Montgomery, J. A., Jr.; Peralta, J. E.; Ogliaro, F.; Bearpark, M. J.; Heyd, J. J.; Brothers, E. N.; Kudin, K. N.; Staroverov, V. N.; Keith, T. A.; Kobayashi, R.; Normand, J.; Raghavachari, K.; Rendell, A. P.; Burant, J. C.; Iyengar, S. S.; Tomasi, J.; Cossi, M.; Millam, J. M.; Klene, M.; Adamo, C.; Cammi, R.; Ochterski, J. W.; Martin, R. L.; Morokuma, K.; Farkas, O.; Foresman, J. B.; Fox, D. J., *Gaussian 16*, Revision A.03, 2016.

30. C. J. Cramer, *Essentials of Computational Chemistry: Theories and Models*, John Wiley & Sons, Chichester, 2nd edn., 2004.
31. A. D. Becke, *Phys. Rev. A*, 1988, **38**, 3098-3100.
32. A. D. Becke, *J. Chem. Phys.*, 1993, **98**, 5648-5652.
33. G. Scalmani, M. J. Frisch, B. Mennucci, J. Tomasi, R. Cammi and V. Barone, *J. Chem. Phys.*, 2006, **124**, 094107.
34. K. Lashgari, R. Norrestam and B. Akermark, *Acta Crystall. C*, 1999, **55**, UC9900108.
35. T. Sato, Y. Hamada, M. Sumikawa, S. Araki and H. Yamamoto, *Ind. Eng. Chem. Res.*, 2014, **53**, 19331-19337.
36. C. Tejel, M. A. Ciriano, M. P. del Río, F. J. van den Bruele, D. G. H. Hetterscheid, N. Tsichlis i Spithas and B. de Bruin, *J. Am. Chem. Soc.*, 2008, **130**, 5844-5845.
37. C. Tejel, M. P. del Río, M. A. Ciriano, E. J. Reijerse, F. Hartl, S. Záliš, D. G. H. Hetterscheid, N. Tsichlis i Spithas and B. de Bruin, *Chem. Eur. J.*, 2009, **15**, 11878-11889.
38. S. Panda, A. Singha Hazari, M. Gogia and G. K. Lahiri, *Inorg. Chem.*, 2020, **59**, 1355-1363.
39. S. Panda, S. K. Bera, P. Goel, A. K. Dutta and G. K. Lahiri, *Inorg. Chem.*, 2019, **58**, 11458-11469.
40. R. Matheu, A. Ghaderian, L. Francàs, P. Chernev, M. Z. Ertem, J. Benet-Buchholz, V. S. Batista, M. Haumann, C. Gimbert-Suriñach, X. Sala and A. Llobet, *Chem. Eur. J.*, 2018, **24**, 12838-12847.
41. T. Kojima, K. Nakayama, K. Ikemura, T. Ogura and S. Fukuzumi, *J. Am. Chem. Soc.*, 2011, **133**, 11692-11700.
42. R. Matheu, M. Z. Ertem, C. Gimbert-Suriñach, J. Benet-Buchholz, X. Sala and A. Llobet, *ACS. Cat.*, 2017, **7**, 6525-6532.
43. R. Matheu, M. Z. Ertem, M. Pipelier, J. Lebreton, D. Dubreuil, J. Benet-Buchholz, X. Sala, A. Tessier and A. Llobet, *ACS. Cat.*, 2018, **8**, 2039-2048.
44. R. Matheu, M. Z. Ertem, C. Gimbert-Suriñach, X. Sala and A. Llobet, *Chem. Rev.*, 2019, **119**, 3453-3471.
45. S. E. Diamond, G. M. Tom and H. Taube, *J. Am. Chem. Soc.*, 1975, **97**, 2661-2664.
46. J. R. Pladziewicz, J. A. Broomhead and H. Taube, *Inorg. Chem.*, 1973, **12**, 639-643.
47. B. S. Tovrog, S. E. Diamond and F. Mares, *J. Am. Chem. Soc.*, 1979, **101**, 5067-5069.
48. A. I. Nguyen, R. G. Hadt, E. I. Solomon and T. D. Tilley, *Chem. Sci.*, 2014, **5**, 2874-2878.

49. L. Duan, F. Bozoglian, S. Mandal, B. Stewart, T. Privalov, A. Llobet and L. Sun, *Nat. Chem.*, 2012, **4**, 418.
50. L. Wang, L. Duan, B. Stewart, M. Pu, J. Liu, T. Privalov and L. Sun, *J. Am. Chem. Soc.*, 2012, **134**, 18868-18880.